



Contents lists available at ScienceDirect

Free Radical Biology and Medicine

journal homepage: www.elsevier.com/locate/freeradbiomed

Advanced photodynamic therapy with an engineered M13 phage targeting EGFR: Mitochondrial localization and autophagy induction in ovarian cancer cell lines

Barbara Bortot^a, Maura Apollonio^a, Gabriele Baj^b, Laura Andolfi^c, Luisa Zupin^a, Sergio Crovella^d, Matteo di Giosia^e, Andrea Cantelli^e, Roberto Saporetti^e, Luca Ulfo^f, Annapaola Petrosino^f, Giovanni Di Lorenzo^a, Federico Romano^a, Giuseppe Ricci^{a,g}, Maurizio Mongiat^h, Alberto Danielli^f, Matteo Calvaresi^{e,*}, Stefania Biffi^{a,**}

^a Institute for Maternal and Child Health, IRCCS Burlo Garofolo, Trieste, Italy

^b BRAIN Center for Neuroscience, Department of Life Sciences, University of Trieste, Trieste, Italy

^c Consiglio Nazionale delle Ricerche, Istituto Officina dei Materiali IOM-CNR, Trieste, Italy

^d Department of Biological and Environmental Sciences, College of Arts and Sciences, University of Qatar, Doha, Qatar

^e Dipartimento di Chimica "G. Ciamician", Alma Mater Studiorum - Università di Bologna, Bologna, Italy

^f Dipartimento di Farmacia e Biotecnologie, Alma Mater Studiorum - Università di Bologna, Bologna, Italy

^g Department of Medical, Surgical and Health Sciences, University of Trieste, Trieste, Italy

^h Department of Research and Diagnosis, Division of Molecular Oncology, Centro di Riferimento Oncologico di Aviano (CRO) IRCCS, Italy

ARTICLE INFO

Keywords:

PDT
EGFR
M13 bacteriophage
Ovarian cancer
Autophagy
Mitochondrial localization

ABSTRACT

Photodynamic therapy (PDT) is a potential synergistic approach to chemotherapy for treating ovarian cancer, the most lethal gynecologic malignancy. Here we used M13 bacteriophage as a targeted vector for the efficient photodynamic killing of SKOV3 and COV362 cells. The M13 phage was refactored (M13_r) to display an EGFR binding peptide in its tip that is frequently overexpressed in ovarian cancer. The refactored phage was conjugated with chlorin e6 (Ce6), one of the most widely used photosensitizers (M13_r-Ce6). The new platform, upon irradiation, generated ROS by type I mechanism and showed activity in killing SKOV3 and COV362 cells even at concentrations in which Ce6 alone was ineffective. A microscopy analysis demonstrated an enhanced cellular uptake of M13_r-Ce6 compared to free Ce6 and its mitochondrial localization. Western blot analysis revealed significant downregulation in the expression of EGFR in cells exposed to M13_r-Ce6 after PDT. Following PDT treatment, autophagy induction was supported by an increased expression of LC3II, along with a raised autophagic fluorescent signal, as observed by fluorescence microscopy analysis for autophagosome visualization. As a conclusion we have herein proposed a bacteriophage-based receptor targeted photodynamic therapy for EGFR-positive ovarian cancer.

1. Introduction

Ovarian cancer (OC) is the most lethal gynecologic malignancy [1]. Due to the relatively asymptomatic nature of the early-stage disease, most of the patients are diagnosed at an advanced degree after cancer has disseminated within the peritoneal cavity [2]. The standard treatment for advanced OC is based on the combination of surgical cytoreduction and paclitaxel/carboplatin combination chemotherapy [3,4].

However, disease recurrence occurs in most patients due to platinum chemotherapy resistance, and a significant effort is needed to identify the best ways this challenge could be effectively addressed. The innovative oncological strategy often combines different therapeutic modalities, offering potential improvements over a single treatment [5–7]. In this context, photodynamic therapy (PDT) is a potential synergistic approach to chemotherapy for the residual disease [8].

PDT involves the uptake of a photosensitizer (PS) followed by

* Corresponding author.

** Corresponding author.

E-mail addresses: matteo.calvaresi3@unibo.it (M. Calvaresi), stefania.biffi@burlo.trieste.it (S. Biffi).

<https://doi.org/10.1016/j.freeradbiomed.2021.11.019>

Received 20 September 2021; Received in revised form 10 November 2021; Accepted 17 November 2021

Available online 19 November 2021

0891-5849/© 2021 The Authors.

Published by Elsevier Inc.

This is an open access article under the CC BY-NC-ND license

(<http://creativecommons.org/licenses/by-nc-nd/4.0/>).

exposure to light of an appropriate wavelength, leading to the photochemical generation of reactive cytotoxic oxygen species [8]. Reactive oxygen species (ROS) are involved in various physiological and pathological processes [9], and multiple cancer therapies nowadays rely on oxidative stress to damage cancer cells [10–12]. PDT-mediated tumor destruction involves three distinct mechanisms [13]: (i) generation of oxidative stress that can directly cause apoptosis, autophagy or necrosis of cancer cells; (ii) destruction of cancer-associated vasculature, leading to tumor infarction; (iii) activation of an acute inflammatory and induction of host-defense immune response that can consequently kill cancer cells. Since ovarian cancer is confined within the peritoneal cavity in most cases, the disease is amenable to regionally localized PDT [14,15]. However, the accumulation of PSs outside tumor lesions and inadequate light dosimetry induce organ toxicity in the peritoneum, with cutaneous phototoxicity and bowel perforation as the primary complication [16,17]. Since the goal of therapeutic precision remains elusive, there is a critical need to develop a targeted PSs formulation that selectively accumulates in tumor lesions, limiting the phototoxicity to the irradiated regions [16]. In this context, nanotechnology disclosed the possibility of engineering new vehicles to deliver drugs or new therapeutic agents targeting ovarian cancer cells [18,19].

Epidermal growth factor receptor (EGFR) is an integral surface receptor mediating external signaling from an entire family of regulatory signals [20]. Interaction of these extracellular signaling molecules with EGFR induces activation of several intracellular pathways such as RAS/MAPK(ERK), PI3K/AKT/mTOR, and JAK/STAT, leading to proliferation, apoptosis inhibition, and cell survival [21]. Of interest, EGFR activation contributes to epithelial-mesenchymal transition, and mutations in this gene and its upregulated expression are often associated with cancer emergence and progression [22,23]. EGFR represents one of the most promising receptors for targeted therapy and several EGFR-targeted therapeutics have been widely used in clinical practice [24]. For instance, anti-EGFR monoclonal antibodies such as cetuximab, panitumumab, and nimotuzumab, hinder natural ligands from binding the EGFR and prevent activation of the receptor tyrosine kinase. However, despite exhibiting upregulated expression of EGFR, a significant part of OC patients do not respond to the anti-EGFR antibodies and inhibitors that entered the clinical setting [8,25].

The development of resistance to EGFR therapy has been attributed to a variety of cellular mechanisms, while the structure of the receptors often remains unchanged. Unlike conventional EGFR therapy, the EGFR targeted PDT treatment does not need an intrinsic effector function. This offer the possibility of continuing to use a target-therapy against EGFR (also for resistant cells) destroying the cancer cells with physical mechanisms (ROS generation), which are able to overcome the cellular adaptations that bestow resistance. Thus, EGFR targeted PDT may represent a promising complementary therapeutic approach for EGFR-positive cancer patients, particularly for those resistant to the available treatments.

The use of viral nanoparticles in PDT has significantly expanded the range of applications of this laser-based therapy [26]. This study employs the M13 bacteriophage as a targeted vector for the efficient photodynamic killing of two different OC cell lines. The M13 phage is refactored (M13_r) to display in its tip an EGFR binding peptide [27,66]. The refactored phage is conjugated with chlorin e6 (Ce6), one of the most widely used photosensitizers (M13_r-Ce6) [28].

2. Materials and methods

2.1. Synthesis and characterization of refactored M13 phages

The SYPIPDT coding sequence was generated by annealing oligonucleotide AD0127 (CATGGCCAGCTATCCGATTCCGGATACCGGTGGC GGTG) and AD0128 (GATCCACCGCCACCGGTATCCGGAATCGGATAGCTGGC). This insert was cloned as a NcoI-BamHI fragment in a pSEX81 vector (ProGen), linearized with the same restriction enzymes,

generating pPK15. Positive clones were verified by sequencing. Clones of *E. coli* TG1 carrying the verified pPK15 phagemid were superinfected with Hyperphage (ProGen) and grown overnight in LB medium supplemented with appropriate antibiotics and 0.4 mM IPTG to promote phage production and induce expression of the fusion construct from the *P_{lac}* promoter of pPK15, enabling multivalent display of the SYPIPDT peptide on the phage tip. After bacterial pelleting, the supernatant containing the M13_r phages was stirred for 90 min at 4 °C in the presence of PEG 8000 and NaCl (SigmaAldrich, respectively 4% and 3% w/v). Next, the solution was centrifuged for 30 min at 20.000 g to precipitate the phages. M13_r virions were resuspended in phosphate-buffered saline pH7.4 and quantified using a UV-Vis spectrophotometer, measuring the absorbance at 269 nm ($\epsilon = 3.84 \text{ cm}^2 \text{ mg}^{-1}$).

2.2. Conjugation of chlorin e6 (Ce6) to the refactored M13 phages

Carboxylic groups of Ce6 were activated to succinimidyl ester derivatives before conjugation with phages. Ce6 was dissolved in DMSO to obtain a concentration of 10 mM. Then solid NHS and EDC were added under stirring to the Ce6 solution, obtaining a final concentration of 45 mM and 30 mM. The solutions were incubated at 25 °C under constant shaking at 700 rpm (ThermoMixer HC, S8012-0000; STARLAB, Hamburg, Germany) for 3 h in dark conditions. 50 μl of activated Ce6 were added, in a dropwise manner, to 1 ml of M13_r 40 nM ($2.4 \cdot 10^{13}$ virions/ml) dissolved in PBS, obtaining a final concentration of 0.5 mM. The mixture was then incubated overnight at 25 °C under continuous shaking (700 rpm). The M13_r-Ce6 bioconjugate was purified by dialysis. Unreacted Ce6 and small molecular weight byproducts of the cross-linking reaction were removed by dialysis in 100 mM sodium carbonate buffer (pH 9) using a regenerated cellulose membrane (14,000 kDa cut-off). The purification process was monitored, performing UV-Vis spectra of the dialysate.

2.3. Conjugation of TRITC to the refactored M13 phages

A stock solution of 10 mM TRITC dissolved in DMSO was prepared. A volume of 50 μl of the stock solution was added dropwise to 1 ml of M13_r 40 nM ($2.4 \cdot 10^{13}$ virions/ml) dissolved in 100 mM sodium carbonate buffer (pH 9). The mixture was then incubated overnight at 25 °C under continuous shaking (700 rpm). Purification process by dialysis was performed to remove the TRITC excess.

2.4. Determination of the ROS generation ability of the M13_r-Ce6 bioconjugate

2.4.1. Detection of singlet oxygen generation

Singlet oxygen emission spectra were recorded with an Edinburgh FLS920 spectrofluorimeter equipped with a Ge detector for emission in the NIR spectral region. These steady-state phosphorescence spectra were acquired with an emission cut-off filter at 850 nm to eliminate artefacts. Correction of the emission spectra for detector sensitivity in the 1200–1400 nm spectral region was performed.

2.4.2. Amplex® red assay

50 mM phosphate buffer at pH 7.4 (PB) was prepared using Milli-Q water. 1 ml of this solution was added to 10 μl of 50 mM of Amplex Red (AR) dissolved in DMSO to obtain a final concentration of 500 μM . Then, 10 μl of 0.4 mg/ml of HRP dissolved in PBS was added to the AR solution to produce the final working solution. The assay was performed using different concentrations of photosensitizers, i.e., Ce6 and M13_r-Ce6 (10, 5, 2, 1, and 0.5 μM). The samples were transferred on a 96-well plate and irradiated for 30 min with a visible light lamp (Valex cold white LED lamp) with an irradiance on the cell plate of 20 mW/cm², measured with a photo-radiometer Delta Ohm LP 471 RAD. 10 μl of AR working solution was added to each sample after the irradiation. Solutions were incubated for 30 min at room temperature in dark conditions,

and then absorbance was measured at 560 nm. The absorbance values were converted to the concentration of peroxides generated upon irradiation, applying a calibration curve produced using standard solutions of H₂O₂.

2.5. Cell cultures

The human ovarian cancer cell line SKOV3 was purchased from ATCC (American Type Culture Collection, Manassas, Virginia United States). The COV362 cell line was kindly provided by Dr Maurizio Mongiat (from Centro di Riferimento Oncologico di Aviano (CRO), IRCCS Aviano Italy). SKOV3-luc cells were maintained in RPMI medium (Thermo Fischer Scientific, Waltham, Massachusetts, USA) supplemented with 10% fetal bovine serum (Euroclone, Milan, Italy) and 1% penicillin/streptomycin antibiotics (Euroclone, Milan, Italy). SKOV3 were made bioluminescent cells (SKOV3-luc), as in detail previously described [18]. The COV362 growing medium was DMEM (Euroclone, Milan, Italy) added with 2 mM of glutamine and 10% fetal bovine serum. All ovarian cancer cell cultures were incubated at 37 °C in a humidified incubator with 5% CO₂.

2.6. Photodynamic treatment

Cells were seeded at a density of 5×10^3 cells/well in 96-multiwell plates (Sarstedt, Nümbrecht, Germany) for cell viability assay and density 3×10^5 cells/well in 6-multiwell plates (Sarstedt, Nümbrecht, Germany) for Western blot analysis. After 24 h, the medium was removed from the plate, and adherent cells were incubated for 90 min with PS (Ce6, and M13-Ce6) at a concentration ranging from 0.05 μM to 2 μM in DMEM medium supplemented with 2.5% FBS. Following incubation, the conditioned medium was removed, and the cells were washed with 1X PBS (Euroclone, Milan, Italy) to eliminate the excess of PS. The cells were maintained in 1X PBS during irradiation. Plates were irradiated with a class IV diode laser (K-Laser Cube series, K-laser d.o.o., Sežana, Slovenia), with emission wavelength at 660 nm, power emission 0.1 W, fluence 2.25 J/cm², irradiance 0.05 W/cm², continuous wave. The device was equipped with an adapted prototype probe specifically designed by Eltech S.r.l. [29], to allow homogeneous irradiation of the wells. After the laser treatment, cells were washed with PBS and maintained in the appropriate medium during post-treatment time (24 h). Control experiments were performed as follows: i) cells were cultured in the same conditions without irradiation or PS exposure (control); ii) cells were cultured in the same conditions and exposed to light (phototoxicity); iii) cells were exposed to the PS without irradiation (dark toxicity), and iv) cells were exposed to the M13_r phage at the corresponding concentration used in the PDT experiments (phage toxicity). Preliminary investigations were conducted to optimize the experimental conditions described above, using different incubation mediums for PSs and different irradiation doses.

2.7. Cytotoxicity assays

After 24 h from the treatments, SKOV3-luc cell viability was assessed using the ONE-GloTmLuciferase Assay System kit (Promega Madison, USA) as previously described [18]. CellTox™ Green Cytotoxicity Assay kit (Promega Madison, WI) was employed to measure cytotoxicity in COV362. According to the manufacturer's instructions, the fluorescence produced by the green dye binding to the dead-cell DNA was determined by the Glomax MultiDetection System instrument (Promega Madison, WI), and the measured relative fluorescent unit (RFU) was proportional to cytotoxicity.

2.8. Western blots

3×10^5 cells were collected and suspended in TUC buffer (7 M urea, 2 M thiourea, 4% CHAPS, 40 mM Tris) with protease inhibitor cocktail

(2 mM PMSF; 1 mM EDTA; 1 mM NaF; 1 mM benzamidine) and was then sonicated for about 10 s. Lysates were then centrifuged at 12,000 g at 4 °C for 10 min, supernatants collected, and protein concentration quantified with Bradford assay. The samples were prepared using Laemli buffer and then boiled at 83 °C for 3 min. 60 μg of proteins were loaded on 12% SDS-PAGE at a voltage of 200 V for about 40 min. Gel proteins were then transferred to a nitrocellulose membrane (Merck) previously wetted with 1X Transfer Buffer. A constant electric current of 300 mA was applied for 90 min. The protein transfer was ascertained by Ponceau Red stain (Merck). Nitrocellulose membranes were incubated with 5% dry milk solution in TBS-Tween 0.05%, except for the analysis of p-mTOR, for which membranes were incubated with a 5% BSA solution for 2 h at room temperature. Next, incubation with primary antibodies was carried out overnight at 4 °C. The following primary antibodies have been used: Cocktail Apoptosis kit (Ab136812, Abcam); Mouse monoclonal anti-human EGFR (sc-373746-HRP, Santa Cruz); Recombinant Anti-LC3B antibody (ab192890, Abcam); P-mTOR (sc-293133, Santa Cruz); Anti-Heme oxygenase-1 (sc-136960HRP, Santa Cruz). After primary antibody incubation, membranes were washed three times for 10 min with TBS-Tween 0.05% and then incubated with secondary antibody (anti-mouse 1:3.000 in TBS-Tween 0.05%) for 1.30 h at 4 °C. In order to develop the membranes, Clarity max Western ECL Substrate (Bio-Rad) was adopted. The kit is composed of Peroxidase Buffer and Luminol, and to develop the immunochemical signal and signals were detected using the CCD-camera-based imager ChemiDoc MP (Bio-Rad). Quantification of bands was performed with Image Studio Lite: Western Blot Analysis Software.

2.9. Cell imaging

SKOV3-luc and COV362 cells were seeded at a density of 1×10^5 at 24 multiwell plates (Sarstedt, Germany) and exposed 24 h later to PDT treatment. Cells were stained with fluorescent probe MitoTracker® Red CMXRos (Invitrogen Thermo Fisher Scientific, Waltham, Massachusetts, USA) at a concentration of 200 nM at 37 °C for 30 min. CYTO-ID Green Detection Reagent 2 (ENZO, Switzerland) was used to stain autophagosome accumulations following the manufacturer's instructions. COV362 positive control of autophagy was obtained by adding starvation medium (Earle's Balanced Salts buffer with 40 μM Chloroquine) to cell culture for 4 h. SKOV3 positive control of autophagy was performed by adding 500 nM of Rapamycin in a complete medium of 24 h. Adherent cells were fixed with paraformaldehyde (PFA) 4% and protected with coverglass mounted using Vectashield mounting medium with DAPI (Vector Laboratories Inc. Burlingame, CA). The fluorescent images were captured using Cytation 5 cell imaging multi-mode reader with objective lens 10× and 20× and processed by GEN5 software (BioTek, Germany). The stained cells were evaluated with a Nikon C1si. Confocal microscope Nikon C1si contains 457,477, 488, 514 nm argon laser lines and 408, 561, 640 nm diode lasers. Laser lights at 488 and 561 nm wavelength were delivered to the sample with an 408/488/561/640 dichromatic reflector using a line lambda protocol to avoid bleed-through of green fluorescence in red channel. Only Plan Apo objectives were used 20× and 60X and detection was performed using separated PMTs for the 515 nm and 590 nm light peaks. The system was operated with a pinhole size of one Airy disk. Electronic zoom was kept at minimum values to reduce potential bleaching. The confocal microscope and the acquisition protocols were inserted using the company proprietary software, NIS Elements C, version 5.0. A series of optical images, acquired at 250 nm increments along the "z" were processed for z-projection and for illustration purposes by using ImageJ (NIH, Bethesda, USA).

2.10. Cellular uptake assay

2.5×10^5 cells were seeded on a microscope glass slide, and cells were exposed to free Ce6 or M13_r-Ce6 for 1.5 h incubation time.

Afterward, the medium was removed, and samples were washed with PBS and stained with DAPI and Mitotraker-green. The prepared samples were analyzed by an inverted microscope (Axiovert 200, Carl Zeiss, Germany), a 63× objective immersion oil (Zeiss, Switzerland), Olympus XM10 camera, and X-Cite fluorescence lamp illuminator (Excelitas Technologies) for visualization of DAPI and MitoTraker Green. For MitoTraker, an excitation bandpass filter (450–490 nm), beam splitter (520 nm), and emission by a lowpass filter (515 nm) were used. Instead, Ce6 was excited with a 405 nm LED (100 mW), beam splitter at 580 nm, and the red fluorescence emission was collected by a lowpass filter (590 nm). The use of the LED allowed for exciting the Ce6 molecules selectively.

2.11. Statistical analysis

Student's t-test and one-way analysis of variance (ANOVA) followed by Tukey's HSD post-hoc test were performed to determine significant differences for two-way or more than two groups, and a *P*-value less than 0.05 was considered significant.

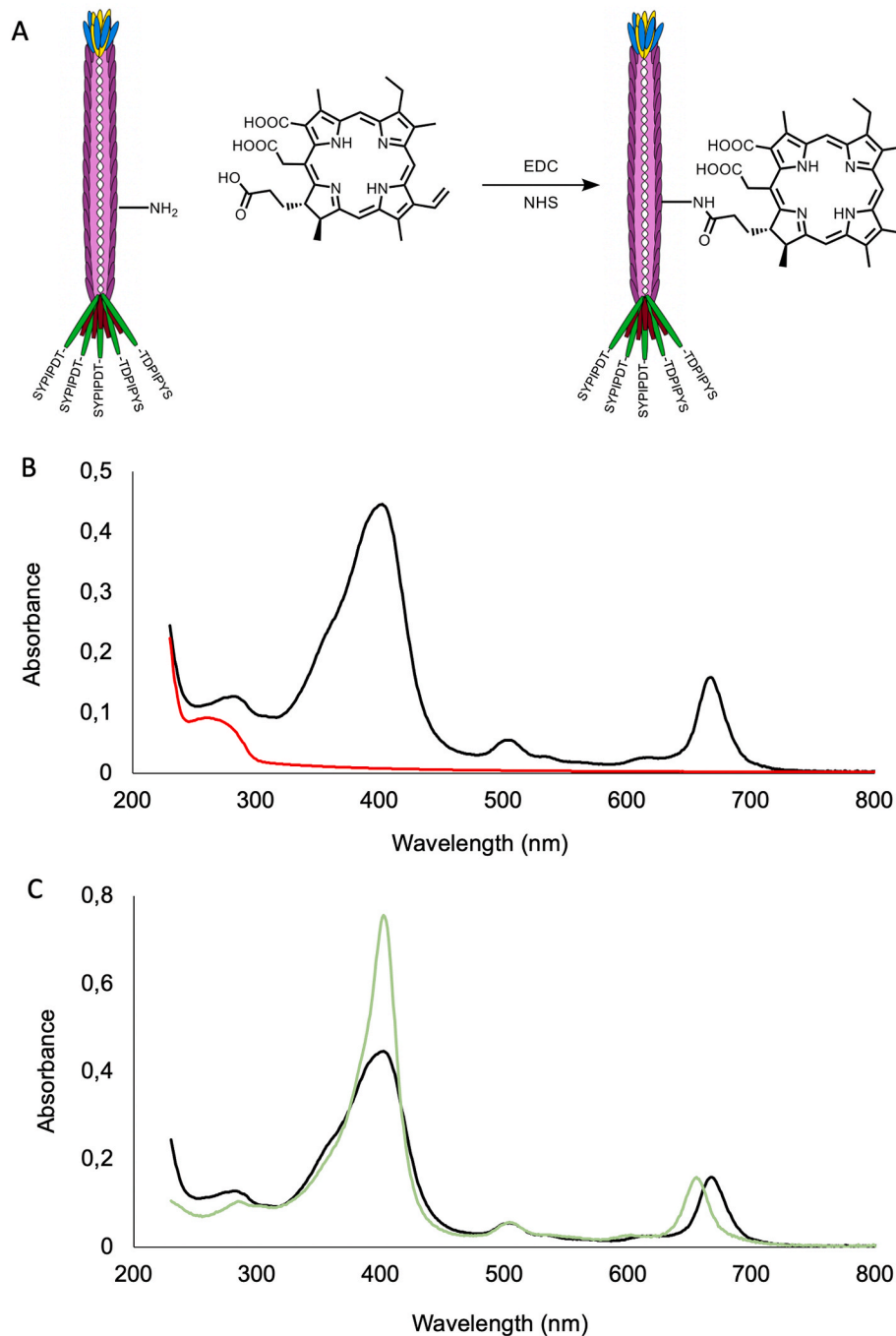


Fig. 1. A) Conjugation of Ce6 to M13r. B) Absorption spectra of M13r (red line) and M13r-Ce6 (black line). C) Normalized (on the lowest energy transition) absorption spectra of Ce6 (green line) and M13r-Ce6 (black line). (For interpretation of the references to color in this figure legend, the reader is referred to the Web version of this article.)

3. Results and discussion

3.1. Engineered phage conjugated with chlorin e6 (Ce6) generates ROS by type I mechanism upon irradiation

M13 phage is a filamentous structure composed of ~2700 copies of the α -helical major coat protein pVIII, symmetrically arranged around the viral DNA to compose an ~880 nm long and ~6.5 nm large supra-molecular assembly. Four other minor coat proteins, pIII, pVI, and pVII, pIX, about 5 copies each, plug the virion, respectively, at the two distal ends. The chemical biology of the M13 phage can be boosted by the incredible ease of molecular manipulation of its genome, allowing it to display proteins and peptides of interest on the phage. The EGFR peptide ligand SYPIPDT [27] was genetically fused to the minor coat protein pIII, generating a recombinant M13_r phage vector able to be internalized by OC cells. A bioconjugate of M13_r with Ce6 was synthesized via EDC/NHS cross-coupling reaction (Fig. 1A) between the carboxylic-acid group of Ce6 and primary amines available for conjugation on the capsid surface (N-terminus and a Lys residue exposed on the viral surface of the pVIII protein) [30]. The total number of conjugation sites available is ~5400 per virus. Absorption spectra of the purified M13_r-Ce6 bioconjugate displayed the diagnostic peaks, characteristic of Ce6 (Fig. 1B), i.e., the Soret band around 400–410 nm and the Q bands in the range 650–670 nm. Considering the initial concentration of M13_r phage and the molar extinction coefficient of Ce6 at 660 nm, approximately 1600 Ce6 molecules were conjugated per M13_r phage, a number in line with the results obtained previously in the conjugation of similar molecules to wild-type M13 phages [31].

The absorbance peak of the most intense Q bands shifted to 668 nm (the typical absorbance in Ce6 is at 655 nm) and the Soret band around 400 nm became broader following conjugation with M13_r (Fig. 1C). These changes in the absorption spectra confirmed that Ce6 was attached to M13_r.

Upon light absorption, Ce6 can produce ROS via two different pathways. In the type II mechanism (energy transfer), singlet oxygen ($^1\text{O}_2$) is generated by the quenching of the excited state of the PS by molecular oxygen ($^3\text{O}_2$). In type I mechanism, a radical species is produced by electron transfer from (or to) the excited state of the photosensitizer. These radical species readily respond to molecular oxygen, forming different reactive oxygen species (ROS), such as hydroxyl radicals and organic hydroperoxides. Spectrofluorimetric measurements are employed to verify the occurrence of the two mechanisms.

The amount of singlet oxygen generated during visible light irradiation was determined directly by measuring the near-infrared phosphorescence at ~1270 nm emitted by $^1\text{O}_2$. The measurement of the near-infrared luminescence of singlet oxygen for two solutions of Ce6 and M13_r-Ce6 (Fig. 2A, inset) at the same concentration showed that the ability of Ce6 to produce $^1\text{O}_2$ disappears upon conjugation with the phage.

The result is not surprising because we already observed that the non-covalent conjugation of Ce6 in proteins strongly reduces the production of $^1\text{O}_2$ [32]. In addition, it is well-known that binding/conjugation of photosensitizers with proteins determines a decrease of $^1\text{O}_2$ generation and an increase of peroxide production, disfavoring the type II mechanism and enhancing the type I mechanism [32–34].

For this reason, we evaluated quantitatively also the generation of peroxides by Ce6 and M13_r-Ce6 bioconjugate, using the Amplex Red assay. A significant improvement in the peroxide production of the M13_r-Ce6 bioconjugate was observed compared to the same concentration of Ce6 (~200%) in all the investigated range (Fig. 2B).

A sacrificial electron donor is generally required to activate the type I mechanism. Electron-rich environments increase photoactivation switch from type II to type I mechanisms [35], which significantly increases the generation of peroxides (electron transfer process) over singlet oxygen production (energy transfer process). The protein residues of the phage can participate directly in the electron transfer reactions [36–38]. Therefore, the type I mechanism is self-activated in the M13_r-Ce6 bioconjugate due to the presence of the protein itself [36–38].

3.2. M13_r-Ce6 exhibits enhanced cellular uptake compared to free Ce6 and co-localized with mitochondria

Cellular uptake and subcellular distribution of photosensitizers are the leading determinants of their cell-killing efficacy [39]. As previously reported, Ce6 incorporates into the plasma membrane and is then internalized in vesicular structures by absorptive endocytosis resulting in an endosome/lysosomal localization [40]. To compare the cellular uptake of M13_r-Ce6 with free Ce6 and determine the targeted agent's subcellular distribution, we performed a microscopy analysis on the SKOV3 and COV362 cell lines. Both cell lines were exposed for 1.5 h to the photosensitizer solution (according to our PDT treatment protocol) at a concentration of 2 μM and then fixed. Ce6 fluorescence intensity was much more robust in cells treated with M13_r-Ce6 than the cells treated with free Ce6 (Fig. 3A). Furthermore, Ce6 fluorescence in the cytoplasm of the cells treated with M13_r-Ce6 overlaid the green fluorescence of MitoTracker labeling. These results indicate that cells internalize Ce6 more slowly than M13_r-Ce6, which co-localized with mitochondria. To confirm the results, we analyzed the intracellular distribution of M13_r labeled with another dye (Fig. 3B). We have chosen the fluorescence dye TRITC for its spectral properties suitable for a co-localization study with the MitoTracker's dye. The stain of the internalized M13_r-TRITC was clearly visible in mitochondria-rich area of the cells. In particular we confirmed, at the high magnification provided by confocal imaging, the colocalization of the M13_r-TRITC red fluorescence with green labeled mitochondria.

The critical aspects in the development of a new photosensitizer include solubility, stability, and effective targeting [41,42]. In this regard, nanoplatforms functionalized with specific receptor-based

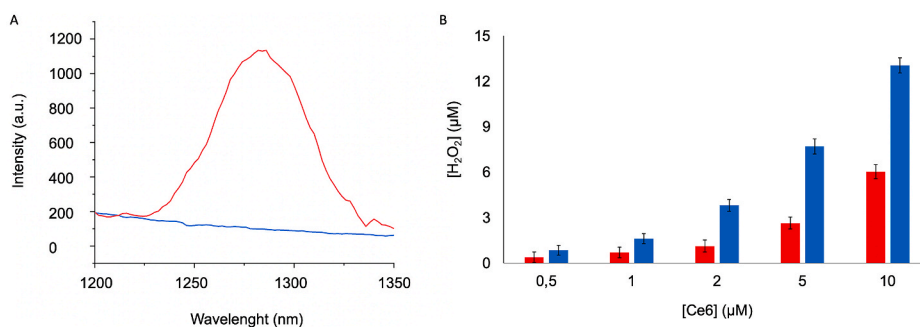


Fig. 2. A) Emission spectra from singlet oxygen generated upon excitation at 660 nm for isoconcentration solutions of Ce6 (red line) and M13_r-Ce6 (blue line). B) Generation of peroxides using different concentrations of Ce6 (red) and M13_r-Ce6 (blue). (For interpretation of the references to color in this figure legend, the reader is referred to the Web version of this article.)

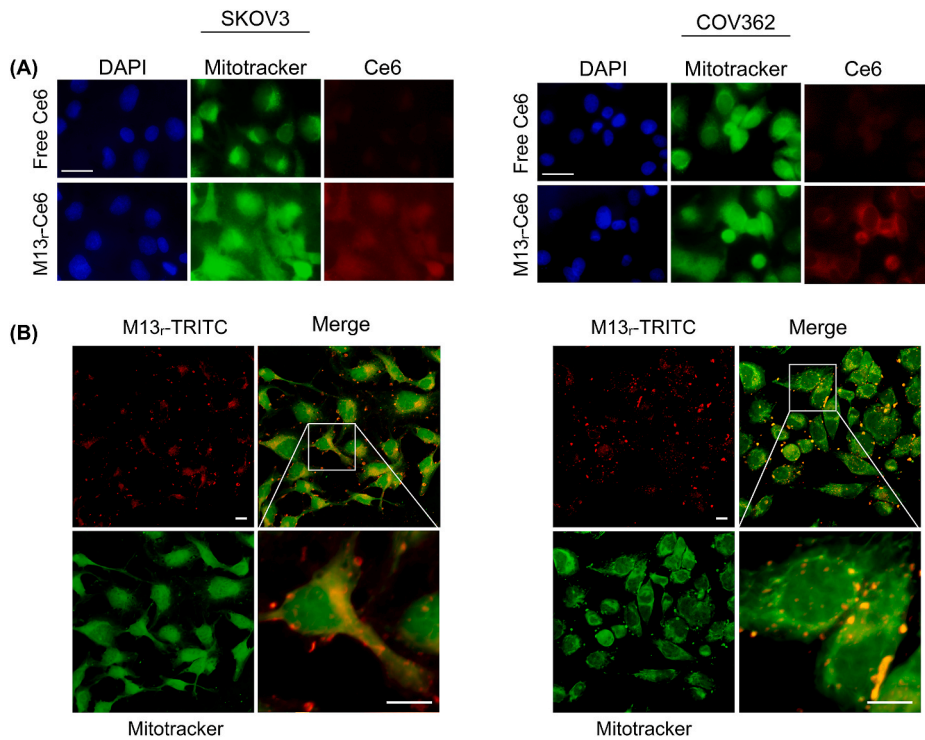


Fig. 3. (A) Fluorescence microscopy images of the Ce6 and M13r-Ce6 cellular uptake by SKOV3 and COV362 cells. We incubated cells with equivalent concentrations (2 μM) of Ce6 and M13r-Ce6 for 1.5 h and co-stained them with fluorescent dyes that label the mitochondria (Mito-Tracker). The first column represents DAPI, the second column Mito-Tracker green labeling, and the third column the Ce6 fluorescence emission of the free Ce6 and M13r-Ce6 conjugated treated cells. Scale bar 50 μm. (B) Confocal fluorescence microscopy images of the M13r-TRITC cellular uptake by SKOV3 and COV362 cells. We incubated cells with M13r-TRITC 2 μM for 1.5 h and co-stained them with Mito-Tracker. Each panel shows representative images of M13r-TRITC (red channel), mitochondria (green channel) in the cells, merge of the two staining and a close-up image. Scale Bar = 10 μm. (For interpretation of the references to color in this figure legend, the reader is referred to the Web version of this article.)

targeting agents could improve cancer cell-specific delivery of photosensitizers. In this study, the M13 phage was refactored to display in its tip an EGFR binding peptide that is frequently overexpressed in ovarian cancer [25,41]. The microscopic study demonstrated an enhanced cellular uptake of M13r-Ce6 compared to free Ce6 and also revealed the distribution of the refactored phage at the mitochondrial level, an interesting factor as it is known to improve the efficacy of PDT in terms of cell killing [34,43].

The mitochondrial accumulation of M13r-Ce6 is also in line with recent research indicating that EGFR not only specifically localizes to the plasma membrane but is also found in the nucleus and within other organelles, such as endosomes, lysosomes, and mitochondria [44].

3.3. M13r-Ce6 exhibits prominent photo-cytotoxicity effect on SKOV3 and COV362 cells

The primary aim of this study was to explore M13r-Ce6 potential as a pharmacological approach to improve Ce6 efficiency. To this end, we evaluated the photodynamic activity of M13r-Ce6 and its results in terms of cell death compared to free Ce6 in two ovarian cancer cell lines, SKOV3 and COV362. SKOV3 cells stably expressing luciferase (SKOV3-luc) were generated as previously described [18]. SKOV3-luc cells were exposed to different concentrations of Ce6, M13r phage, M13r-Ce6 for 1.5 h, irradiated with a dose of 2.25 J/cm², and viability was evaluated by luciferin assay after 24 h. As shown in Fig. 4, the viability analysis displayed a significant cytotoxic activity in the cells treated with M13r-Ce6 in a dose-dependent manner.

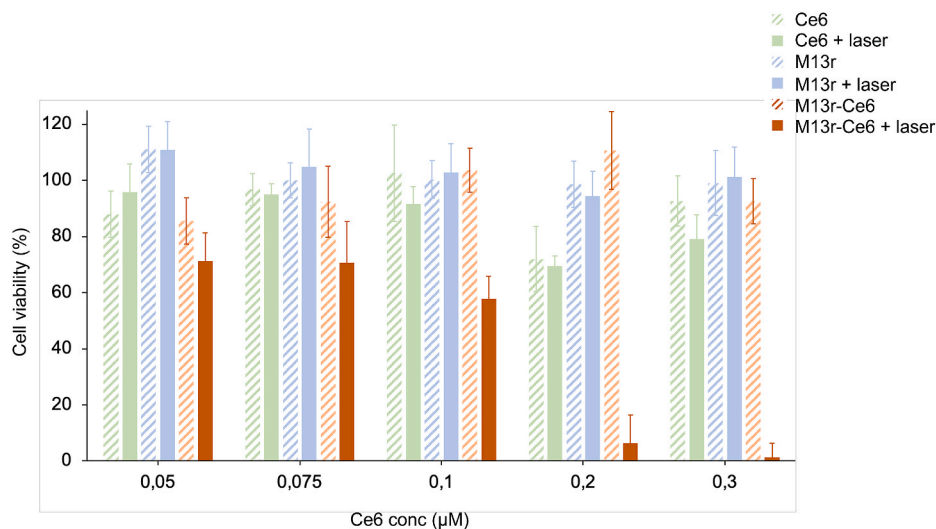


Fig. 4. Cytotoxic effect of M13r-Ce6 and PDT on SKOV3-luc cells. Cells were incubated with M13r phage, Ce6 and M13r-Ce6, at different concentrations for 1.5 h, then irradiated with a dose of 2.25 J/cm². Analysis was performed 24 h after incubation. Data are shown as mean ± SD of 3 individual experiments.

In the whole range of concentration used, the p-value corresponding to the F-statistic of one-way ANOVA with $\alpha = 0.05$ was lower than 0.01, strongly suggesting that one or more pairs of treatments were significantly different. We had six treatments (Ce6 dark and laser, M13r dark and laser, and M13r-Ce6 dark and laser), for which we applied Tukey's HSD test to pinpoint which of them exhibited statistically significant differences. Whereas there were no statistically significant differences between Ce6 dark and laser, and M13r dark and laser, the treatment with M13r-Ce6 laser was statistically different from all the other treatments.

At concentration of Ce6 0.05 μM to Ce6 0.3 μM , we observed a decrease in cell viability from 71% (p-value = 0.0015, difference between the control and treatment group by Student's t-test) to 1% (p-value = 7.00226E-19, difference between the control and treatment group by Student's t-test). In the same concentration range, cells treated with free Ce6 revealed a decrease in cell viability from 96% (p-value = 0.0008, difference between the control and treatment group by Student's t-test) to 79% (p-value = 0.0262, difference between the control and treatment group by Student's t-test). We could not observe any toxic effect for the M13_r phage in the investigated concentration range.

We employed Western blot analysis to delineate phenotypic changes of the SKOV3-luc cells and analyze a panel of markers after the exposure at two different concentrations of M13_r-Ce6 (Fig. 5A). Analysis was performed with M13_r-Ce6 at concentrations Ce6 0.05 μM and Ce6 0.2 μM , which showed respectively 71% (p-value = 0.0015, difference between the control and treatment group by Student's t-test) and 6% (p-value = 2.66628E-13, difference between the control and treatment group by Student's t-test) of cell viability. We examined the oxidative stress-associated marker Heme oxygenase-1, the targeted receptor EGFR, the marker of autophagy LC3B, the key regulator of protein synthesis and cell proliferation mTOR, and the apoptosis marker procaspase-3. Heme oxygenase-1 (HO-1) is responsible for heme groups' oxidative cleavage to carbon monoxide (CO), biliverdin, and ferrous iron. It has been reported that HO-1 expression is highly increased by stressful conditions and is significantly induced by PDT, suggesting an essential role in cytoprotection against PDT-mediated damage [45]. In our experimental condition, after 24 h of laser irradiation, HO-1 protein levels were undetectable in the SKOV3 control cells and became detectable in the cell samples treated with M13_r-Ce6 (Ce6 0.2 μM) (Fig. 5A). Our results are consistent with previous findings that indicate that PDT may induce HO-1 expression via reactive oxygen species production [46].

As exposed in Fig. 5A, we observed a significant downregulation in the expression of EGFR in SVOK3 cells exposed to M13_r-Ce6 (Ce6 0.2 μM) 24 h after laser irradiation concerning EGFR expression in the control groups, which is consistent with an EGFR degradation when cell viability was significantly affected [47].

Many significant advances in platinum-resistance biomarkers have

recently come to light, providing evidence that activation of EGFR related signaling pathways was correlated with cisplatin-resistance in OC cells [48,49]. However, despite some encouraging preclinical results and the presence of several EGFR-targeted therapeutics available in the clinic (including monoclonal antibodies and tyrosine kinase inhibitors), this approach demonstrated minimal clinical efficacy in terms of progression-free or overall survival in the treatment of patients with OC, and intensive research has now focused on identifying factors related to the resistance phenomenon [8,25]. Since EGFR-targeted PDT treatment does not need an intrinsic effector function, this may represent a promising complementary therapeutic approach for EGFR-positive cancer patients, particularly for those resistant to the available treatments. In this context, the ability of irradiated M13_r-Ce6 to down-regulate the expression of EGFR in OC cell lines is extremely interesting due to i) direct oxidative damage induced by the refactored phages than binds EGFR (EGFR-targeted PDT) [50] or ii) redox-dependent regulation of EGFR signaling [51,52]. Among clinical investigations on EGFR targeted therapy in OC, recent results suggest that the extent of EGFR degradation predicts the antitumor effect in colorectal cancer and correlates better with an EGFR inhibitor (cetuximab) treatment efficacy than the initial number of EGFRs on the cell surface [53].

Western blot analysis of procaspase-3 from cells after 24 h of laser irradiation was negative for active caspase-3, indicating the lack of apoptosis induction (Fig. 5A). However, autophagic cell death after PDT treatment was suggested by an increase of LC3II, which coincided with a decrease of p-mTOR expression after the exposure at the higher M13_r-Ce6 concentration (Ce6 0,2 μM). The results are consistent with previous findings proving that initiation of autophagosomes formation is regulated by mTOR inhibition [54], and the induction of autophagy in PDT protocols can occur independently of an apoptotic outcome [55]. Moreover, mitochondrial and ER-localized photosensitizers cause selective photodamage to some proteins (i.e., m-TOR) involved in the apoptotic/autophagic process. Of interest, Shi and colleagues demonstrated that cardamomin-induced autophagy is associated with glycolysis inhibition via mTOR inhibition in SKOV3 cells [56].

Overall, Western blot analyses of whole-cell lysates revealed significant protein expression changes among samples undergoing PDT with M13_r-Ce6 at a concentration Ce6 0,2 μM , suggesting intracellular ROS generation and a PDT killing mechanism based on autophagy. It has been demonstrated that ROS generation [57] and PDT treatment can induce autophagy [58].

Therefore, to further explore the killing mechanisms due to M13_r-Ce6 irradiation, we subsequently performed a fluorescence imaging analysis at the same concentration. Cells were analyzed by fluorescence microscopy to evaluate the appearance of autophagosomes following treatment with light (Fig. 5B). To assess autophagy, we used CYTO-ID® Autophagy Detection Kit 2.0 based on a dye that selectively labels accumulated autophagic vacuoles, exhibiting bright fluorescence upon

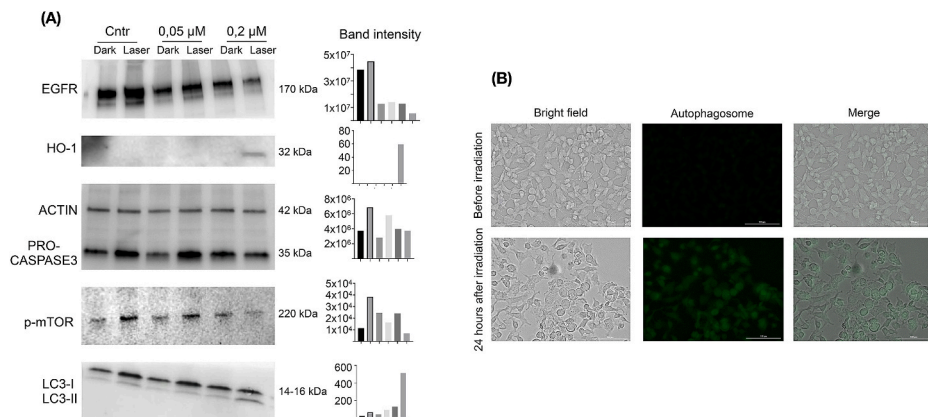


Fig. 5. (A) Western blot analysis following PDT of the targeted receptor EGFR, the oxidative stress-associated marker Heme oxygenase-1, the marker of autophagy LC3B-II, the key regulator of protein synthesis and cell proliferation mTOR, and the apoptosis marker procaspase-3. (B) Representative fluorescence microscopy images of SKOV3-luc cells before and after irradiation. After 24 h of laser irradiation, cells were labeled with CYTO-ID® Green. All the fluorescent images were captured using Cytation5 cell imaging multi-mode reader with objective lens 20 \times , followed by uniform processing using Cytation5 software (bar = 100 μm). (For interpretation of the references to color in this figure legend, the reader is referred to the Web version of this article.)

incorporation into pre-autophagosomes, autophagosomes, and autolysosomes (autophagolysosomes). The bright-field and fluorescence images are shown in Fig. 5B, where an increase in autophagic fluorescent signal can be seen in cells treated with M13_r-Ce6 after laser irradiation compared with the low background in control samples.

To further explore M13_r-Ce6 and PDT's effect on OC cells, we performed a similar analysis on the cell line COV362. This OC cell line behaves differently than SKOV3, and after 24 h of treatment, most of the cells had detached from the culture plate. We, therefore, decided to study protein expression by western blotting and autophagosome formation by fluorescence 2 h after treatment. The viability analysis displayed a significant cytotoxic activity in the cells treated with M13_r-Ce6 in a dose-dependent manner, consistent with results obtained with SKOV3-luc (Supplementary Information Fig. 1). We could not observe any toxic effect for Ce6 and M13_r phage in the investigated concentration range. At the lowest concentrations of Ce6 0.2 μM and Ce6 0.05 μM, the p-value corresponding to the F-statistic of one-way ANOVA with $\alpha = 0.05$ was higher than 0.05, suggesting that treatments were not significantly different. At the highest concentrations of Ce6 0.5 μM and Ce6 1 μM, instead, the p-value corresponding to the F-statistic of one-way ANOVA with $\alpha = 0.05$ was lower than 0.01, strongly suggesting that one or more pairs of treatments were significantly different. Again, the Tukey's HSD pinpointed the treatment with M13_r-Ce6 laser statistically different from all the other treatments.

We employed Western blot analysis to analyze a panel of markers after the exposure at two different concentrations of M13_r-Ce6 (Supplementary Information Fig. 2). Analysis was performed at Ce6 0.5 μM and Ce6 1 μM, which showed respectively 64% (p-value = 0.0001766, difference between the control and treatment group by Student's t-test) and 23% (p-value = 0.001139, difference between the control and treatment group by Student's t-test) of cell viability.

At both concentrations, we noted a significant downregulation in the expression of EGFR also in COV362 cells after 2 h of laser irradiation than the expression of EGFR present in the control groups (cells before irradiation), which is consistent with an EGFR degradation. Western blot analysis of procaspase-3 from cells after 2 h of laser irradiation was negative for active caspase-3. Autophagic cell death after PDT treatment was suggested by an increase of LC3II.

The study improved the autophagosome formation imaging in cells with altered morphology at an early point upon irradiation. The bright-field and fluorescence imaging of autophagy are shown in Fig. 6. An increase in autophagic fluorescent signal can be seen in the early response of cells to irradiation compared with the low background in control samples, along with altered morphology. Analysis was

performed at Ce6 0.5 μM and Ce6 1 μM, and the increase in autophagic fluorescent signal was dose-dependent.

M13_r-Ce6 exhibited a prominent photo-cytotoxicity effect on two ovarian cancer cell lines associated with mitochondrial localization. As an organelle particularly sensitive to photodamage, mitochondria represent one of the most effective sites of action to kill cells using PDT [39]. These results support the idea that targeting specific organelles involves modulation of cell death pathways and amplifying photo-therapeutic outcomes.

Autophagy induction were suggested by an increased expression of LC3II and an expansion in autophagic fluorescent signal through fluorescence microscopy analysis for visualizing autophagosomes. The link between autophagy and cancer has gained much interest in recent years. Excessive cellular autophagy levels might lead to autophagic cell death (type II programmed cell death) in cancers [59]. Cancer cells' final life/death threshold decision is influenced by the interplay of autophagy and apoptosis, which depends on the class, concentration, exposure of cytotoxic agents, and the type of cancer cells. Reactive oxygen species (ROS) concurrently prompt apoptosis and autophagy processes, but the relationship between these molecular responses must be fully elucidated [46,55,60,61].

We believe that our current data might strengthen the notion that autophagy can occur independently of apoptosis in PDT protocols [55] and suggest an important role of mitochondria-located EGFR in autophagy [62].

4. Conclusions

In this study, the M13 phage was refactored to display in its tip an EGFR binding peptide. The refactored phage was then conjugated with Ce6, one of the most widely used photosensitizers, generating an innovative phototheranostic platform for cancer imaging and treatment [63–65]. The M13_r-Ce6 bioconjugates, upon irradiation, generated ROS by type I mechanism. The new platform showed activity in killing SKOV3 and COV362 ovarian cancer cells even at concentrations in which Ce6 alone is ineffective in inhibiting tumor growth. The mitochondrial localization of these systems and the induction of autophagy represent an intriguing finding, as the role of EGFR located in the mitochondria in the autophagy process is still largely unexplored.

Funding

This research was funded by the Ministry of Health "5% anno 2016" Grant to IRCCS Burlo Garofolo, P.I. Biffi Stefania, project title: "A

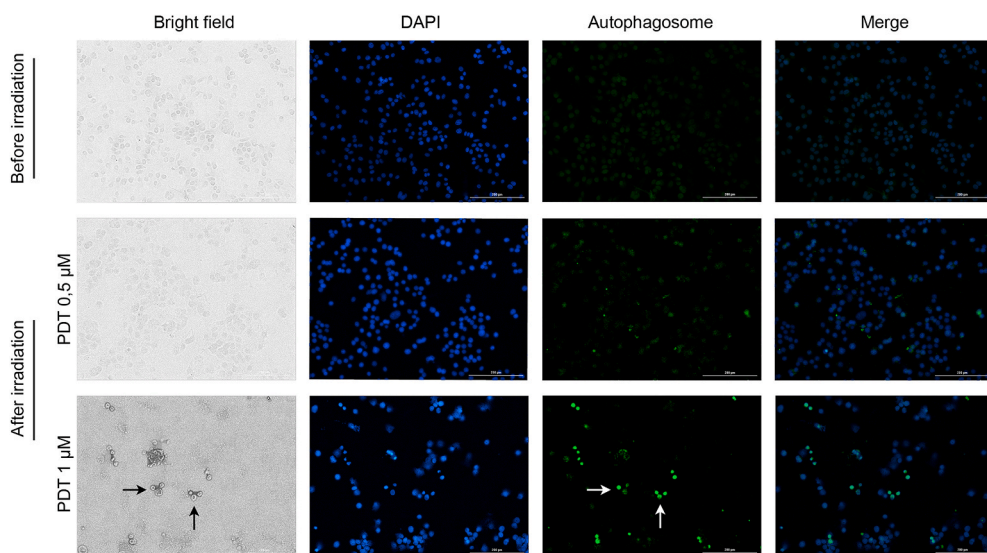


Fig. 6. Autophagy induction after PDT treatment in COV362 cells. Representative fluorescence microscopy images of COV362 cells before and after irradiation. After 2 h of laser irradiation, cells were labeled with DAPI and CYTO-ID® Green. DAPI staining was carried out to visualize cell nuclei, which appear in blue, while phagosomes appear in green (bar = 200 μm). Black arrows in bright field indicate altered cellular morphology, white arrows the corresponding autophagic fluorescence signal. All the fluorescent images were captured using Cytation5 cell imaging multi-mode reader with objective lens 10× (bar = 200 μm), followed by uniform processing using Cytation5 software. (For interpretation of the references to color in this figure legend, the reader is referred to the Web version of this article.)

preclinical platform from human ovarian cancer cells to investigate potential cisplatin resistance markers.” MDG was supported by a FIRC-AIRC fellowship for Italy (id. 22318). The research leading to these results has received funding from AIRC under MFAG 2019 - ID. 22894 project – P.I. Calvaresi Matteo.

Declaration of competing interest

The authors declare no conflict of interest.

Data availability statement

The raw/processed data required to reproduce the above findings cannot be shared at this time due to technical/time limitations. Data available on request from the authors.

Acknowledgments

We thank Dr. Martina Bradascia for the English revision of the manuscript. A part of the images in this paper were generated in the Light Microscopy Imaging Center (LMIC) of the University of Trieste at the Life Sciences Department, funded as detailed at www.units.it/confocal.

Appendix A. Supplementary data

Supplementary data to this article can be found online at <https://doi.org/10.1016/j.freeradbiomed.2021.11.019>.

References

- [1] Y. Zhang, G. Luo, M. Li, P. Guo, Y. Xiao, H. Ji, Y. Hao, Global patterns and trends in ovarian cancer incidence: age, period and birth cohort analysis, *BMC Cancer* 19 (2019) 984, <https://doi.org/10.1186/s12885-019-6139-6>.
- [2] Z. Nash, U. Menon, Ovarian cancer screening: current status and future directions, *Best Pract. Res. Clin. Obstet. Gynaecol.* 65 (2020) 32–45, <https://doi.org/10.1016/j.bpobgyn.2020.02.010>.
- [3] A.A. Wright, K. Bohlke, D.K. Armstrong, M.A. Bookman, W.A. Cliby, R.L. Coleman, D.S. Dizon, J.J. Kash, L.A. Meyer, K.N. Moore, A.B. Olawaiye, J. Oldham, R. Salani, D. Sparacio, W.P. Tew, I. Vergote, M.I. Edelson, Neoadjuvant chemotherapy for newly diagnosed, advanced ovarian cancer: society of gynecologic oncology and American society of clinical oncology clinical practice guideline, *J. Clin. Oncol.* 34 (2016) 3460.
- [4] I. Vergote, C.G. Tropé, F. Amant, G.B. Kristensen, T. Ehlen, N. Johnson, R.H. M. Verheijen, M.E.L. van der Burg, A.J. Lacave, P.B. Panici, G.G. Kenter, A. Casado, C. Mendiola, C. Coens, L. Verleye, G.C.E. Stuart, S. Pecorelli, N.S. Reed, Neoadjuvant chemotherapy or primary surgery in stage IIIC or IV ovarian cancer, *N. Engl. J. Med.* 363 (2010) 943–953, <https://doi.org/10.1056/NEJMoa0908806>.
- [5] A.J. Cortez, P. Tudrej, K.A. Kujawa, K.M. Lisowska, Advances in ovarian cancer therapy, *Cancer Chemother. Pharmacol.* 81 (2018) 17–38, <https://doi.org/10.1007/s00280-017-3501-8>.
- [6] E. Kozłowska, T. Vallius, J. Hynninen, S. Hietanen, A. Färkkilä, S. Hautaniemi, Virtual clinical trials identify effective combination therapies in ovarian cancer, *Sci. Rep.* 9 (2019) 18678, <https://doi.org/10.1038/s41598-019-55068-z>.
- [7] Q.Y. Meng, H.L. Cong, H. Hu, F.-J. Xu, Rational design and latest advances of codelivery systems for cancer therapy, *Mater. Today Bio.* 7 (2020) 100056, <https://doi.org/10.1016/j.mtbio.2020.100056>.
- [8] S. Nath, M.A. Saad, M. Pigula, J.W.R. Swain, T. Hasan, Photoimmunotherapy of ovarian cancer: a unique niche in the management of advanced disease, *Cancers* 11 (2019) 1887, <https://doi.org/10.3390/cancers11121887>.
- [9] K.B. Kennel, F.R. Greten, Immune cell - produced ROS and their impact on tumor growth and metastasis, *Redox Biol.* 42 (2021) 101891, <https://doi.org/10.1016/j.redox.2021.101891>.
- [10] C. Hegedűs, K. Kovács, Z. Polgár, Z. Regdon, É. Szabó, A. Robaszkievicz, H. J. Forman, A. Martner, L. Virág, Redox control of cancer cell destruction, *Redox Biol.* 16 (2018) 59–74, <https://doi.org/10.1016/j.redox.2018.01.015>.
- [11] M. Yusupov, A. Privat-Maldonado, R.M. Cordeiro, H. Verswyvel, P. Shaw, J. Razzokov, E. Smits, A. Bogaerts, Oxidative damage to hyaluronan-CD44 interactions as an underlying mechanism of action of oxidative stress-inducing cancer therapy, *Redox Biol.* 43 (2021), <https://doi.org/10.1016/j.redox.2021.101968>, 101968.
- [12] G. Manda, G. Isvoranu, M.V. Comanescu, A. Manea, B. Debeleac Butuner, K. S. Korkmaz, The redox biology network in cancer pathophysiology and therapeutics, *Redox Biol.* 5 (2015) 347–357, <https://doi.org/10.1016/j.redox.2015.06.014>.
- [13] A.P. Castano, P. Mroz, M.R. Hamblin, Photodynamic therapy and anti-tumour immunity, *Nat. Rev. Cancer* 6 (2006) 535–545, <https://doi.org/10.1038/nrc1894>.
- [14] M.Q. Almerie, G. Gossedge, K.E. Wright, D.G. Jayne, Treatment of peritoneal carcinomatosis with photodynamic therapy: systematic review of current evidence, *Photodiagnosis Photodyn. Ther.* 20 (2017) 276–286, <https://doi.org/10.1016/j.pdpdt.2017.10.021>.
- [15] S.K. Hendren, S.M. Hahn, F.R. Spitz, T.W. Bauer, S.C. Rubin, T. Zhu, E. Glatstein, D. L. Fraker, Phase II trial of debulking surgery and photodynamic therapy for disseminated intraperitoneal tumors, *Ann. Surg. Oncol.* 8 (2001) 65–71, <https://doi.org/10.1007/s10434-001-0065-x>.
- [16] S. Xu, A.-L. Bulin, A. Hurbin, H. Elleaume, J.-L. Coll, M. Broekgaarden, Photodynamic diagnosis and therapy for peritoneal carcinomatosis: emerging perspectives, *Cancers* 12 (2020) 2491, <https://doi.org/10.3390/cancers12092491>.
- [17] R.L. Yanovsky, D.W. Bartenstein, G.S. Rogers, S.J. Isakoff, S.T. Chen, Photodynamic therapy for solid tumors: a review of the literature, *Photodermatol. Photoimmunol. Photomed.* 35 (2019) 295–303, <https://doi.org/10.1111/phpp.12489>.
- [18] B. Bortot, M. Mongiat, E. Valencic, S.D. Monego, D. Licastro, M. Crosera, G. Adami, E. Rampazzo, G. Ricci, F. Romano, G.M. Severini, S. Biffi, Nanotechnology-based cisplatin intracellular delivery to enhance chemo-sensitivity of ovarian cancer, *Int. J. Nanomed.* 15 (2020) 4793, <https://doi.org/10.2147/IJN.S247114>.
- [19] G. Di Lorenzo, G. Ricci, G.M. Severini, F. Romano, S. Biffi, Imaging and therapy of ovarian cancer: clinical application of nanoparticles and future perspectives, *Theranostics* 8 (2018) 4279–4294, <https://doi.org/10.7150/thno.26345>.
- [20] A.A. Rosenkranz, T.A. Slastnikova, Epidermal growth factor receptor: key to selective intracellular delivery, *Biochem. Moscow* 85 (2020) 967–993, <https://doi.org/10.1134/S0006297920090011>.
- [21] Y. Yarden, G. Pines, The ERBB network: at last, cancer therapy meets systems biology, *Nat. Rev. Cancer* 12 (2012) 553–563, <https://doi.org/10.1038/nrc3309>.
- [22] S. Lamouille, J. Xu, R. Derynck, Molecular mechanisms of epithelial-mesenchymal transition, *Nat. Rev. Mol. Cell Biol.* 15 (2014) 178–196, <https://doi.org/10.1038/nrm3758>.
- [23] S. Sigismund, D. Avanzato, L. Lanzetti, Emerging functions of the EGFR in cancer, *Mol. Oncol.* 12 (2018) 3–20, <https://doi.org/10.1002/1878-0261.12155>.
- [24] R. Zeineldin, C.Y. Muller, M.S. Stack, L.G. Hudson, Targeting the EGF receptor for ovarian cancer therapy, *J. Oncol.* 2010 (2010) 414676, <https://doi.org/10.1155/2010/414676>.
- [25] E. Teplinsky, F. Muggia, EGFR and HER2: is there a role in ovarian cancer? *Transl. Cancer Res.* 4 (2015) 107–117, <https://doi.org/10.21037/3934>.
- [26] S. Lin, C. Liu, X. Han, H. Zhong, C. Cheng, Viral nanoparticle system: an effective platform for photodynamic therapy, *Int. J. Mol. Sci.* 22 (2021) 1728, <https://doi.org/10.3390/ijms22041728>.
- [27] M. Hamzeh-Mivehroud, A. Mahmoudpour, S. Dastmalchi, Identification of new peptide ligands for epidermal growth factor receptor using phage display and computationally modeling their mode of binding, *Chem. Biol. Drug Des.* 79 (2012) 246–259, <https://doi.org/10.1111/j.1747-0285.2011.01282.x>.
- [28] R.R. Allison, G.H. Downie, R. Cuenca, X.-H. Hu, C.J. Childs, C.H. Sibata, Photosensitizers in clinical PDT, *Photodiagnosis Photodyn. Ther.* 1 (2004) 27–42, [https://doi.org/10.1016/S1572-1000\(04\)00007-9](https://doi.org/10.1016/S1572-1000(04)00007-9).
- [29] L. Zupin, G. Ferri, P.M. Tricarico, R. Gratton, C. Nait-Meddour, G. Ottaviani, S. Crovella, Impact of 970 nm photobiomodulation therapy on wound healing in cellular models of hidradenitis suppurativa, *Laser Med. Sci.* 36 (2020) 691–698, <https://doi.org/10.1007/s10103-020-03097-w>.
- [30] K. Li, Y. Chen, S. Li, H.G. Nguyen, Z. Niu, S. You, C.M. Mello, X. Lu, Q. Wang, Chemical modification of M13 bacteriophage and its application in cancer cell imaging, *Bioconjugate Chem.* 21 (2010) 1369–1377, <https://doi.org/10.1021/bc900405q>.
- [31] Y.S. Nam, T. Shin, H. Park, A.P. Magyar, K. Choi, G. Fantner, K.A. Nelson, A. M. Belcher, Virus-templated assembly of porphyrins into light-harvesting nanoantennae, *J. Am. Chem. Soc.* 132 (2010) 1462–1463, <https://doi.org/10.1021/ja908812b>.
- [32] M. Di Giosia, D. Genovese, A. Cantelli, M. Cingolani, E. Rampazzo, G. Strever, M. Tavoni, N. Zaccaroni, M. Calvaresi, L. Prodi, Synthesis and characterization of a reconstituted myoglobin-chlorin e6 adduct for theranostic applications, *J. Porphyr. Phthalocyanines* 24 (2019) 887–893, <https://doi.org/10.1142/S108842461950202X>.
- [33] A. Cantelli, F. Piro, P. Pecchini, M. Di Giosia, A. Danielli, M. Calvaresi, Concanavalin A-Rose Bengal bioconjugate for targeted Gram-negative antimicrobial photodynamic therapy, *J. Photochem. Photobiol., B* 206 (2020) 111852, <https://doi.org/10.1016/j.jphotobiol.2020.111852>.
- [34] A. Cantelli, M. Malferrari, A. Soldà, G. Simonetti, S. Forni, E. Toscanella, E. J. Mattioli, F. Zerbetto, A. Zanelli, M. Di Giosia, M. Zangoli, G. Barbarella, S. Rapino, F. Di Maria, M. Calvaresi, Human serum albumin-oligothiophene bioconjugate: a phototheranostic platform for localized killing of cancer cells by precise light activation, *JACS Au* 1 (2021) 925–935, <https://doi.org/10.1021/jacsau.1c00061>.
- [35] H. Ding, H. Yu, Y. Dong, R. Tian, G. Huang, D.A. Boothman, B.D. Sumer, J. Gao, Photoactivation switch from type II to type I reactions by electron-rich micelles for improved photodynamic therapy of cancer cells under hypoxia, *J. Contr. Release* 156 (2011) 276–280, <https://doi.org/10.1016/j.jconrel.2011.08.019>.
- [36] A. Soldà, A. Cantelli, M.D. Giosia, M. Montalti, F. Zerbetto, S. Rapino, M. Calvaresi, C60@lysozyme: a new photosensitizing agent for photodynamic therapy, *J. Mater. Chem. B* 5 (2017) 6608–6615, <https://doi.org/10.1039/C7TB00800G>.
- [37] M. Di Giosia, P.H.H. Bomans, A. Bottoni, A. Cantelli, G. Falini, P. Franchi, G. Guarracino, H. Friedrich, M. Lucarini, F. Paolucci, S. Rapino, N.A.J. M. Sommerdijk, A. Soldà, F. Valle, F. Zerbetto, M. Calvaresi, Proteins as supramolecular hosts for C60: a true solution of C60 in water, *Nanoscale* 10 (2018) 9908–9916, <https://doi.org/10.1039/c8nr02220h>.

- [38] M.D. Giosia, A. Soldà, M. Seeger, A. Cantelli, F. Arnesano, M.I. Nardella, V. Mangini, F. Valle, M. Montalti, F. Zerbetto, S. Rapino, M. Calvaresi, V. Ntziachristos, A bio-conjugated fullerene as a subcellular-targeted and multifaceted phototheranostic agent, *Adv. Funct. Mater.* 31 (2021) 2101527, <https://doi.org/10.1002/adfm.202101527>.
- [39] I.R. Calori, H. Bi, A.C. Tedesco, Expanding the limits of photodynamic therapy: the design of organelles and hypoxia-targeting nanomaterials for enhanced photokilling of cancer, *ACS Appl. Bio Mater.* 4 (2021) 195–228, <https://doi.org/10.1021/acsbm.0c00945>.
- [40] H. Mojziso, S. Bonneau, C. Vever-Bizet, D. Brault, Cellular uptake and subcellular distribution of chlorin e6 as functions of pH and interactions with membranes and lipoproteins, *Biochim. Biophys. Acta Biomembr.* 1768 (2007) 2748–2756, <https://doi.org/10.1016/j.bbmem.2007.07.002>.
- [41] S. Biffi, R. Voltan, B. Bortot, G. Zauli, P. Secchiero, Actively targeted nanocarriers for drug delivery to cancer cells, *Expert Opin. Drug Deliv.* 16 (2019) 481–496, <https://doi.org/10.1080/17425247.2019.1604679>.
- [42] S. Biffi, R. Voltan, E. Rampazzo, L. Prodi, G. Zauli, P. Secchiero, Applications of nanoparticles in cancer medicine and beyond: optical and multimodal in vivo imaging, tissue targeting and drug delivery, *Expert Opin. Drug Deliv.* 12 (2015) 1837–1849, <https://doi.org/10.1517/17425247.2015.1071791>.
- [43] Y. Dogra, D.C.J. Ferguson, N.J.F. Dodd, G.R. Smerdon, A. Curnow, P.G. Winyard, The hydroxypyridinone iron chelator CP94 increases methyl-aminolevulinic acid-based photodynamic cell killing by increasing the generation of reactive oxygen species, *Redox Biol.* 9 (2016) 90–99, <https://doi.org/10.1016/j.redox.2016.07.002>.
- [44] W. Han, H.-W. Lo, Landscape of EGFR signaling network in human cancers: biology and therapeutic response in relation to receptor subcellular locations, *Cancer Lett.* 318 (2012) 124–134, <https://doi.org/10.1016/j.canlet.2012.01.011>.
- [45] D. Nowis, M. Legat, T. Grzela, J. Niderla, E. Wilczek, G. Wilczyński, E. Glodkowska, P. Mrówka, T. Issat, J. Dulak, A. Józkowicz, H. Waś, M. Adamek, A. Wrzosek, S. Nazarewski, M. Makowski, T. Stoklosa, M. Jakóbsiak, J. Goła, Heme oxygenase-1 protects tumor cells against photodynamic therapy-mediated cytotoxicity, *Oncogene* 25 (2006) 3365–3374, <https://doi.org/10.1038/sj.onc.1209378>.
- [46] T. Takahashi, S. Misawa, S. Suzuki, N. Saeki, Y. Shinoda, Y. Tsunooka, J. Akimoto, Y. Fujiwara, Possible mechanism of heme oxygenase-1 expression in rat malignant meningioma KMY-J cells subjected to talaporfin sodium-mediated photodynamic therapy, *Photodiagnosis Photodyn. Ther.* 32 (2020) 102009, <https://doi.org/10.1016/j.pdpdt.2020.102009>.
- [47] R. Ebner, R. Derynck, Epidermal growth factor and transforming growth factor- α : differential intracellular routing and processing of ligand-receptor complexes, *Cell Regul.* 2 (1991) 599–612, <https://doi.org/10.1091/mbc.2.8.599>.
- [48] A. Poursheikhani, H. Yousefi, J. Tavakoli-Bazzaz, G. Seyed H, EGFR blockade reverses cisplatin resistance in human epithelial ovarian cancer cells, *Iran, Biomed. J.* 24 (2020) 365–373, <https://doi.org/10.29252/ibj.24.6.365>.
- [49] L. Yang, H. Zhao, X. Yin, H. Liang, Z. Zheng, Q. Shen, W. Hu, Exploring cisplatin resistance in ovarian cancer through integrated bioinformatics approach and overcoming chemoresistance with sanguinarine, *Am. J. Transl. Res.* 12 (2020) 923–939.
- [50] N. Shirasu, S.O. Nam, M. Kuroki, Tumor-targeted photodynamic therapy, *Anticancer Res.* 33 (2013) 2823–2831.
- [51] N. Ahmad, K. Kalka, H. Mukhtar, In vitro and in vivo inhibition of epidermal growth factor receptor-tyrosine kinase pathway by photodynamic therapy, *Oncogene* 20 (2001) 2314–2317, <https://doi.org/10.1038/sj.onc.1204313>.
- [52] D.E. Heppner, A. van der Vliet, Redox-dependent regulation of epidermal growth factor receptor signaling, *Redox Biol.* 8 (2016) 24–27, <https://doi.org/10.1016/j.redox.2015.12.002>.
- [53] Y. Okada, T. Kimura, T. Nakagawa, K. Okamoto, A. Fukuya, T. Goji, S. Fujimoto, M. Sogabe, H. Miyamoto, N. Muguruma, Y. Tsuji, T. Okahisa, T. Takayama, EGFR downregulation after anti-EGFR therapy predicts the antitumor effect in colorectal cancer, *Mol. Cancer Res.* 15 (2017) 1445–1454, <https://doi.org/10.1158/1541-7786.MCR-16-0383>.
- [54] J. Zhang, Teaching the basics of autophagy and mitophagy to redox biologists—mechanisms and experimental approaches, *Redox Biol.* 4 (2015) 242–259, <https://doi.org/10.1016/j.redox.2015.01.003>.
- [55] J.J. Reiners, P. Agostinis, K. Berg, N.L. Oleinick, D. Kessel, Assessing autophagy in the context of photodynamic therapy, *Autophagy* 6 (2010) 7–18, <https://doi.org/10.4161/auto.6.1.10220>.
- [56] D. Shi, D. Zhao, P. Niu, Y. Zhu, J. Zhou, H. Chen, Glycolysis inhibition via mTOR suppression is a key step in cardamonin-induced autophagy in SKOV3 cells, *BMC Compl. Alternative Med.* 18 (2018) 317, <https://doi.org/10.1186/s12906-018-2380-9>.
- [57] E.E. Essick, F. Sam, Oxidative stress and autophagy in cardiac disease, neurological disorders, aging and cancer, *Oxidative Med. Cell. Long.* 3 (2010) 168–177, <https://doi.org/10.4161/oxim.3.3.12106>.
- [58] T. Liu, X. Ma, T. Ouyang, H. Chen, Y. Xiao, Y. Huang, J. Liu, M. Xu, Efficacy of 5-aminolevulinic acid-based photodynamic therapy against keloid compromised by downregulation of SIRT1-SIRT3-SOD2-mROS dependent autophagy pathway, *Redox Biol.* 20 (2019) 195–203, <https://doi.org/10.1016/j.redox.2018.10.011>.
- [59] Y. Tsujimoto, S. Shimizu, Another way to die: autophagic programmed cell death, *Cell Death Differ.* 12 (Suppl 2) (2005) 1528–1534, <https://doi.org/10.1038/sj.cdd.4401777>.
- [60] C. Song, W. Xu, H. Wu, X. Wang, Q. Gong, C. Liu, J. Liu, L. Zhou, Photodynamic therapy induces autophagy-mediated cell death in human colorectal cancer cells via activation of the ROS/JNK signaling pathway, *Cell Death Dis.* 11 (2020) 1–14, <https://doi.org/10.1038/s41419-020-03136-y>.
- [61] W.K. Martins, R. Belotto, M.N. Silva, D. Grasso, M.D. Suriani, T.S. Lavor, R. Itri, M. S. Baptista, T.M. Tsubone, Autophagy regulation and photodynamic therapy: insights to improve outcomes of cancer treatment, *Front. Oncol.* 10 (2021) 3121, <https://doi.org/10.3389/fonc.2020.610472>.
- [62] H. Li, L. You, J. Xie, H. Pan, W. Han, The roles of subcellularly located EGFR in autophagy, *Cell. Signal.* 35 (2017) 223–230, <https://doi.org/10.1016/j.cellsig.2017.04.012>.
- [63] D. Gao, X. Guo, X. Zhang, S. Chen, Y. Wang, T. Chen, G. Huang, Y. Gao, Z. Tian, Z. Yang, Multifunctional phototheranostic nanomedicine for cancer imaging and treatment, *Mater. Today Bio.* 5 (2020) 100035, <https://doi.org/10.1016/j.mtbio.2019.100035>.
- [64] M. Di Giosia, F. Zerbetto, M. Calvaresi, Incorporation of molecular nanoparticles inside proteins: the trojan horse approach in theranostics, *Acc. Mater. Res.* 2 (2021) 594–605, <https://doi.org/10.1021/accountsmr.1c00065>.
- [65] Z. Ouyang, Y. Gao, M. Shen, X. Shi, Dendrimer-based nanohybrids in cancer photomedicine, *Mater. Today Bio.* 10 (2021) 100111, <https://doi.org/10.1016/j.mtbio.2021.100111>.
- [66] Luca Ulfo, et al., Orthogonal nanoarchitectonics of M13 phage for receptor targeted anticancer photodynamic therapy, *Nanoscale* (2021), <https://doi.org/10.1039/D1NR06053H>. In press, <https://pubs.rsc.org/en/content/articlelanding/2021/nr/d1nr06053h>.